

Pulse based Variational Quantum Optimal Control for hybrid quantum computing

R.J.P.T. de Keijzer,¹ O. Tse,¹ and S.J.J.M.F. Kokkelmans¹

¹*Eindhoven University of Technology, P. O. Box 513, 5600 MB Eindhoven, The Netherlands**

(Dated: February 21, 2022)

This work studies pulse based variational quantum algorithms (VQAs), which are designed to determine the ground state of a quantum mechanical system by combining classical and quantum hardware. In contrast to more standard gate based methods, *pulse based methods* aim to directly optimize the laser pulses interacting with the qubits, instead of using some parametrized gate based circuit. Using the mathematical formalism of optimal control, these laser pulses are optimized. This method has been used in quantum computing to optimize pulses for quantum gate implementations, but has only recently been proposed for full optimization in VQAs [1, 2]. Pulse based methods have several advantages over gate based methods such as faster state preparation, simpler implementation and more freedom in moving through the state space [3]. Based on these ideas, we present the development of a novel *adjoint based* variational method. This method can be tailored towards and applied in neutral atom quantum computers. This method of pulse based *variational quantum optimal control* is able to approximate molecular ground states of simple molecules up to chemical accuracy and is able to compete with the gate based variational quantum eigensolver in terms of total number of quantum evaluations. The total evolution time T and the form of the control Hamiltonian H_c are important factors in the convergence behavior to the ground state energy, both having influence on the quantum speed limit and the controllability of the system.

I. INTRODUCTION

Quantum computing is presently in the noisy intermediate-scale quantum (NISQ) era [4], where the available quantum computers cannot outperform their classical counterparts. Nevertheless, even in the NISQ era, quantum computers can be used for specific and well-designed cases [5]. One such application is in solving optimization tasks. In this field, Variational Quantum Algorithms (VQAs) have emerged as the leading optimization technique to obtain quantum advantage on NISQ devices. These algorithms are hybrid, i.e. the algorithm exploits both the classical and quantum computer. Certain VQAs have shown proof of concept for small dimensional problems with various designs of qubits [6–10]. The common aim of these algorithms is to determine the lowest eigenvalue of a quantum Hamiltonian H_{mol} , which can be equated to finding the ground state energy of a molecule. One example of a VQA is the variational quantum eigensolver (VQE), which evolves an initial state through a gate-based quantum logic circuit to prepare an approximate ground state $|\psi_f\rangle$. In recent years, VQE has been implemented on many different qubit systems and has become a highly active area of research (cf. [11, 12] for recent comprehensive overviews).

Generally, in VQAs, the final qubit states $|\psi_f\rangle$ are prepared from an initial state $|\psi_0\rangle$ by a quantum circuit of parametrized gates. These gates can either manipulate a single qubit or multiple qubits at once, and particularly on a neutral atom qubit system, are implemented using specific laser pulses. The pulses necessary to implement

such a gate can be optimized in terms of fidelity, robustness, etc. using the mathematical formalism of optimal control [13–15]. This theory finds its use in quantum algorithms such as GRAPE [16] and CRAB [17]. The entire gate sequence can in principle be seen as a discretization of one continuous laser pulse, as thoroughly explored by Magann et al. [1]. From this stems our idea of Variational Quantum Optimal Control (VQOC) as an alternative to VQE. Instead of optimizing a sequence of parameters of gates, a laser pulse is optimized to construct a state $|\psi_f\rangle$ close to the ground state of a Hamiltonian H_{mol} . This idea has been principally investigated by Meitei et al. [2] and Choquette et al. [3]. The aim of this work is to explore this option more deeply and systematically by developing a theory for VQOC, and to compare our results with the more established VQE method. The main advantages of our pulse-based method are that the pulses provide more flexibility in the evolution of the initial state, allowing for a broader exploration of the state space; the preparation time T can be minimized, mitigating unwanted effects of qubit lifetimes and decoherence. Both of these advantages are especially important in the NISQ era. In this work, we further show how to realistically implement VQOC on a Rydberg atom-based qubit system. From this analysis, we see that VQOC can approximate ground state energies of small molecules up to chemical accuracy [18] on a Rydberg system.

The layout of this paper is as follows. Sec. II describes VQAs in the NISQ era. Sec. III explains the standard VQE method and its shortcomings. In Sec. IV our novel VQOC method is rigorously introduced. In Sec. V the strain on the quantum measurement of both algorithms is described, as well as our method of comparing the algorithms. Finally, Sec. VII shows initial results of VQOC, and compares VQOC to VQE.

* Corresponding author: r.d.keijzer@tue.nl

II. VQAS IN THE NISQ ERA

The aim of a variational quantum algorithm is to evolve an initial qubit state $|\psi_0\rangle \in \mathcal{H}^m := \text{span}(\{|0\rangle, |1\rangle\})^{\otimes m} \simeq \mathbb{C}^{2^m}$ in a given preparation time T , to the ground state $|\psi_g\rangle$ of a problem Hamiltonian $H_{\text{mol}} \in \mathcal{L}(\mathcal{H}^m)$. Here, \mathcal{H}^m is the Hilbert space of m -qubit states, and $\mathcal{L}(\mathcal{H}^m)$ is the Hilbert space of operators on m qubits. The Frobenius inner product on $\mathcal{L}(\mathcal{H}^m)$ is given by

$$\langle A, B \rangle_F = \text{Tr}[A^\dagger B].$$

The state evolution, as with every quantum system, is mediated through the Schrödinger equation, given in propagator formalism as

$$t \in (0, T) : \quad i\partial_t U(t) = H(t)U(t); \quad U(0) = I, \quad (1)$$

where $U(t) \in \mathcal{L}(\mathcal{H}^m)$ is the unitary propagator which describes the evolution of the qubit state as $|\psi(t)\rangle = U(t)|\psi_0\rangle$. The goal of a VQA is thus to manipulate $H(t)$ in a way that makes $U(T)$ map the initial state $|\psi_0\rangle$ to the ground state $|\psi_g\rangle$. To do so, the Hamiltonian $H(t)$ is parametrized, and the variational principle [19] is employed to approximate the ground state. Two important factors in this process are the possible parametrization of the Hamiltonian $H(t)$ and the preparation time T . Figure 1 illustrates the Hilbert space of qubit states.

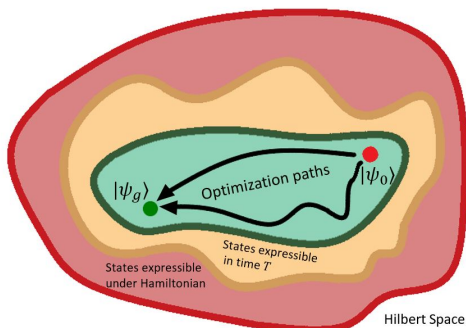


Figure 1: The Hilbert space of qubit states (red) with subsets of the states expressible under the evolution Hamiltonian $H(t)$ (yellow) and the states expressible in preparation time T (green).

The possible Hamiltonians $H(t)$ determine a subset of the Hilbert space that is reachable, e.g. if the initial state is unentangled and there are no interaction terms in $H(t)$, then all entangled states are unreachable. An even smaller subset is the set of states reachable in a finite time T (given a bound on the infinity norm of $H(t)$). The concept of a minimal time necessary to reach a state $|\psi_f\rangle$ is called the *quantum speed limit* (QSL) [20–22].

Several factors are important in creating a NISQ-friendly VQA: (A) the preparation time T should be as small as possible to suppress decoherence effects, (B) a large

portion of Hilbert space should be expressible, so the algorithm can be used to find the ground states of many H_{mol} , and (C) the evolution should be straightforward to implement and control on the quantum computing system. We will argue in Secs. III and IV that our VQOC method adheres to these criteria better than VQE does.

III. VQE

The variational quantum eigensolver, first proposed in a paper by Peruzzo and McClean in 2014 [23], is the most widely implemented VQA to date. Using a parametrized quantum logic circuit, a sequence of quantum gates, it has proven able to closely approximate the ground state of several small molecules [7, 8, 11]. See also cf. [24] for a recent overview of VQE.

In the VQE algorithm, the evolution of the initial qubit state is done via qubit gates. These gates can be described as matrix elements $\mathcal{L}(\mathcal{H}^n)$, where $1 \leq n \leq m$ is the number of qubits the gate acts on. Examples of these gates are $R_X(\theta_x)$ and $R_Z(\theta_z)$ gates, which respectively rotate a qubit around the x -axis by an angle θ_x and z -axis by an angle θ_z on the Bloch sphere (see Fig. 3). Other examples include entangling gates such as the canonical CNOT gate and the SWAP gate. A sequence of parametrized and unparametrized gates together with a set of parameters $\vec{\theta}$ determines the evolution.

One often used template for such a gate sequence alternates between blocks of parametrized single qubit gates $U_{i,j}$, with i indicating the qubit and j the block, and an unparametrized entangling gate U_{ent} (which itself could consist of multiple small gates, such as CNOT gates). The final propagator will take the form

$$U(\vec{\theta}) = \left[U_{\text{ent}} \prod_{q=1}^m U_{q,d}(\vec{\theta}) \right] \cdots \left[U_{\text{ent}} \prod_{q=1}^m U_{q,1}(\vec{\theta}) \right], \quad (2)$$

where the depth d of a state preparation is defined as the number of blocks in the gate sequence. This method is called the hardware-efficient ansatz [25] and is especially relevant in NISQ machines where single qubit gates $U_{q,d}$ can be implemented with high fidelity, and the passive interaction between the qubits can be used to create entanglement gates U_{ent} [4]. If such an interaction is not present and the qubit system possesses some form of control in entanglement operations, then there is more freedom in choosing what U_{ent} should look like, and this choice is highly influential on the outcome of the algorithm [26].

After state preparation, the energy of the prepared state on H_{mol} is determined, which can be done efficiently on a quantum computer for Hamiltonians with sparse decompositions [27]. Based on these measurement outcomes, the set of parameters is updated in order to create a state with lower energy. In VQE, stochastic approaches are

often implemented to update the parameters. One often used example is the simultaneous perturbation stochastic approximation (SPSA) method [6, 28, 29]. This method samples two points in the parameter space close to $\vec{\theta}$ and measures their energies. Based on these results, a step is taken against the direction of an estimated gradient of the energy w.r.t. the parameters. The total number of quantum evaluations (QE) per parameter update is thus given by

$$\#QE = 2 \cdot \#\text{shots}, \quad (3)$$

where $\#\text{shots} = O(\epsilon^{-2})$ is the number of times a measurement is to be repeated in order to get an $O(\epsilon)$ error in the expectation values. Here, one quantum evaluation is equated to one measurement of an expectation value like $\langle \psi | H_{\text{mol}} | \psi \rangle$ (see [30] for more detail).

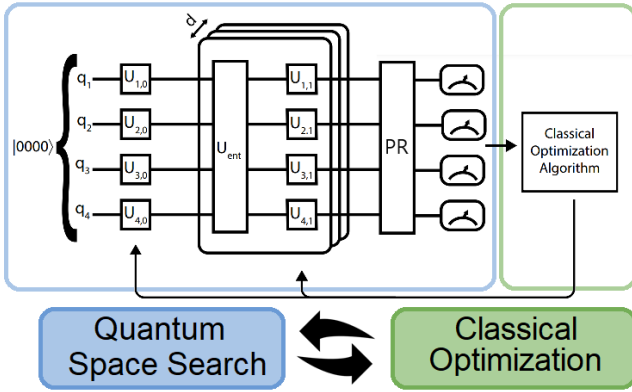


Figure 2: Schematic diagram of VQE illustrating the interplay between quantum space search and classical optimization. An initial state evolves through a hardware-efficient ansatz gate sequence of parametrized gates $U_{i,j}$ and entanglement gates U_{ent} . Afterwards, the state is post-rotated (PR) [31] and measured. A classical optimization algorithm then updates the parameters of the $U_{i,j}$ gates.

When looking at the NISQ-friendly criteria of Sec. II we see that for VQE, the following issues exist:

- (A) The preparation time T is fully determined by the gate sequence and can not be decreased unless the gate sequence is altered (see Fig. 3).
- (B) Even with enough control available, the gate sequence might inhibit the space of reachable states. For example, if the qubits can be fully rotated on the Bloch sphere by the quantum computing system; if only Z-gates were included in the gate sequence a large part of the Hilbert space becomes inaccessible.
- (C) The necessary control to create certain gates might be demanding. For instance, in a Rydberg system, complex and time-consuming laser pulses might be

necessary to create specific single qubit or entanglement gates. Implementation is, therefore, not straightforward.

Based on these shortcomings in VQE, we believe that variational quantum optimal control can serve as a more NISQ-friendly VQA.

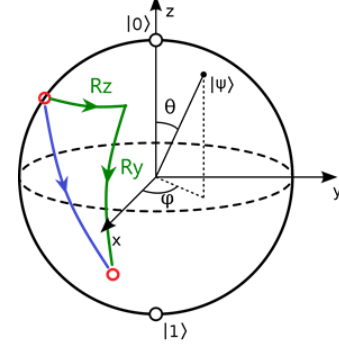


Figure 3: Illustration of NISQ-unfriendliness in VQE. The northern hemisphere state (red dot) needs to be mapped to the southern hemisphere state (red dot). By taking a R_Z gate followed by a R_Y gate, the green path is taken. In terms of technical control, the blue path could have been followed, resulting in faster evolution.

IV. OPTIMAL CONTROL

In this section, the derivation of the pulse-based variational quantum optimal control algorithm (VQOC) as a VQA is given. The motivation for a pulse-based method stems from the idea that every gate is implemented as a laser pulse. Therefore, the entire gate sequence can be seen as a discretization of one continuous laser pulse, as principally explored by Magann et al. [1]. On the other hand, the root of a gate-based quantum logic circuit stems from an analogy to digital computing. In principle, however, there is nothing digital about the outset of VQAs. Therefore, there is also no a priori reason as to why gate-based algorithms would be preferable.

The VQOC algorithm can be used to optimize various types of control functions in the qubit system. In particular, this algorithm can optimize the controllable laser pulses that interact with individual qubits. Because of this, we refer to the control functions as pulses.

The goal in our optimal control setup is to minimize a given functional $J : \mathcal{U} \times \mathcal{Z} \mapsto \mathbb{R}$ subject to the equality constraint $e(U, z) = 0$ for a given map $e : \mathcal{U} \times \mathcal{Z} \mapsto \mathcal{X}^*$ and $z \in \mathcal{Z}_{ad}$ [32]. Here, J is the *cost functional*; $e = 0$ describes the *state equation*; \mathcal{U} , \mathcal{Z} and \mathcal{X} are appropriate function spaces; $\mathcal{Z}_{ad} \subset \mathcal{Z}$ is the set of *admissible pulses*; \mathcal{X}^* is the dual of \mathcal{X} . The problem statement reads

$$\min_{(U,z) \in \mathcal{U} \times \mathcal{Z}_{ad}} J(U, z) \quad \text{s.t.} \quad e(U, z) = 0 \quad \text{in } \mathcal{X}^* \quad (4)$$

In the Lagrangian formulation of Eq. (4), a Lagrange multiplier $P \in \mathcal{X}$ is added to penalize the constraint, i.e.

$$\mathcal{L}(U, z, p) := J(U, z) + \langle P, e(U, z) \rangle_{\mathcal{X}, \mathcal{X}^*}, \quad (5)$$

and the saddle-point problem becomes

$$\min_{(U, z) \in \mathcal{U} \times \mathcal{Z}_{ad}} \max_{P \in \mathcal{X}} L(U, z, P).$$

The necessary conditions for optimality, also called the KKT conditions [33], can thus be reformulated as

$$\begin{aligned} D_P \mathcal{L}(U, z, P) &= 0 \\ D_U \mathcal{L}(U, z, P) &= 0 \\ D_z \mathcal{L}(U, z, P)[\tilde{z} - z] &\geq 0 \quad \forall \tilde{z} \in \mathcal{Z}_{ad}. \end{aligned} \quad (6)$$

We now apply the optimal control formalism to find the ground state energy of a quantum Hamiltonian H_{mol} . We begin with defining the set of admissible pulses. Let $\mathcal{Z} = L^2((0, T); \mathbb{C}^L)$, $L \in \mathbb{N}$, be the Hilbert space of squared-integrable L -dimensional complex-valued functions. For a fixed $z_{\text{max}} \in (0, \infty)$, we set

$$\mathcal{Z}_{ad} = \left\{ z \in \mathcal{Z} \mid \|z\|_\infty := \text{ess sup}_{t \in [0, T]} \sum_{l=1}^L |z_l(t)| \leq z_{\text{max}} \right\}.$$

The space of admissible pulses \mathcal{Z}_{ad} ensures that the physical controls remain realizable. The inner product in \mathcal{Z} is given by

$$\langle \tilde{z}, z \rangle_{\mathcal{Z}} := \sum_{l=1}^L \int_0^T \text{Re} \left[\tilde{z}_l(t) \overline{z_l(t)} \right] dt,$$

with \bar{z} being the complex conjugate of z .

We consider a parametrization of the Hamiltonian $H(t)$ in Eq. (1) of the form

$$H[z(t)] = H_d + H_c[z(t)], \quad z \in \mathcal{Z}_{ad}, \quad (7)$$

where H_d is a drift Hamiltonian representing the passive evolution of the system (see Eq. (9) below), and

$$H_c[z] := \sum_{l=1}^L \left[Q_l z_l + Q_l^\dagger \bar{z}_l \right]$$

is the control Hamiltonian with control operators Q_l , which are not necessarily Hermitian or unitary. Examples of what these control operators could represent are discussed in Sec. V. In the Supplementary Material, we show that the Schrödinger equation of Eq. (1) has well-defined solutions for all admissible pulses. There, it is shown that (1) admits a unique solution $U \in W^{1,2}((0, T); \mathcal{L}(\mathcal{H}^m))$ for every pulse $z \in \mathcal{Z}_{ad}$, where $W^{1,2}$ is the Sobolev space of functions in L^2 having squared-integrable weak derivatives [34]. Based on this result, we choose the spaces

$$\mathcal{U} = \mathcal{X} = W^{1,2}((0, T); \mathcal{L}(\mathcal{H}^m)).$$

\mathcal{U} and \mathcal{X} are Hilbert spaces, with the inner product

$$\langle \tilde{P}, P \rangle_{\mathcal{U}} := \int_0^T \langle \partial_t \tilde{P}(t), \partial_t P(t) \rangle_F + \langle \tilde{P}(t), P(t) \rangle_F dt.$$

The map $e : \mathcal{U} \times \mathcal{Z} \mapsto \mathcal{X}^*$ describing the Schrödinger equation as constraint is then given for all $P \in \mathcal{X}$ by

$$\begin{aligned} \langle P, e(U, z) \rangle_{\mathcal{X}, \mathcal{X}^*} &:= \text{Re}[\langle P(0), U(0) - I \rangle_F] \\ &+ \int_0^T \text{Re}[\langle P(t), i\partial_t U(t) - H[z(t)]U(t) \rangle_F] dt, \end{aligned}$$

which appears also in the Lagrangian formulation of Eq. (5) as the penalization term. Note that this is a duality pairing and not the standard inner product on \mathcal{X} . The solvability of the constraint $e(U, z) = 0$ for each $z \in \mathcal{Z}_{ad}$ gives rise to a solution map $S : \mathcal{Z}_{ad} \mapsto \mathcal{U}$, $S(z) = U$, where U is the unique solution of the Schrödinger equation with Hamiltonian $H[z]$.

For the ground state energy finding problem, we consider the cost functional $J(U, z) = J_1(U) + J_2(z)$, with

$$\begin{aligned} J_1(U) &:= \langle \psi(T) | H_{\text{mol}} | \psi(T) \rangle, \quad |\psi(t)\rangle = U(t) |\psi_0\rangle; \\ J_2(z) &:= \frac{\lambda}{2} \langle z, z \rangle_{\mathcal{Z}}, \quad \lambda > 0, \end{aligned}$$

where $|\psi_0\rangle$ is a fixed initial qubit state. $J_1(U)$, therefore, describes the energy of the state generated by $U(T)$, while the J_2 term punishes for high-energy pulses.

Altogether, we have a well-defined ground state energy finding problem taking the form of Eq. (4), which is shown to admit a minimizer $z_* \in \mathcal{Z}_{ad}$ in the Supplementary Material. In practice, the parameter $\lambda > 0$ in J_2 is chosen to be large, and the third condition in Eq. (6) often reduces to $D_z L(U_*, z_*, P_*) = 0$. In this case, the KKT conditions in Eq. (6) read as follows (the derivations are provided in the Supplementary Material):

$$\begin{aligned} \text{(state equation)} : \quad & i\partial_t U(t) = H[z(t)]U(t), & U(0) &= I, \\ \text{(adjoint equation)} : \quad & i\partial_t P(t) = H[z(t)]P(t), & P(T) &= -2iH_{\text{mol}}|\psi(T)\rangle\langle\psi_0|, \\ \text{(control equation)} : \quad & \lambda z_l(t) - \text{Tr} \left[Q_l^\dagger \left(P(t)U^\dagger(t) + U(t)P^\dagger(t) \right) \right] = 0, & l &= 1, \dots, L. \end{aligned}$$

where $\{\cdot, \cdot\}$ is the anticommutator. It can be verified that the solution $P \in \mathcal{X}$ to the adjoint equation is given explicitly in terms of U as

$$P(t) = -2iU(t)U^\dagger(T)H_{\text{mol}}|\psi(T)\rangle\langle\psi_0|,$$

thereby allowing the second term in the control equation to be expressed as

$$\begin{aligned}\eta_l(t) &:= -\text{Tr}\left[Q_l^\dagger\left(P(t)U^\dagger(t) + U(t)P^\dagger(t)\right)\right] \\ &= \sum_{k=1}^K -2i \left\langle \psi(t) \left| \left[V_{k,l}^\dagger, \Gamma^\dagger(T, t)H_{\text{mol}}\Gamma(T, t) \right] \right| \psi(t) \right\rangle.\end{aligned}$$

where $\Gamma(t, s) := U(t)U^\dagger(s)$ describes the evolution by the pulses from s to t , $[A, B] = AB - BA$ is the usual commutator, and $V_{k,l}$ are unitaries decomposing Q_l as

$$Q_l = \sum_{k=1}^K V_{k,l}, \quad l = 1, \dots, L.$$

These terms can be efficiently determined on a quantum computer by first applying the pulse until time t , using the parameter gradient algorithm [35] (see Supplementary Material), then applying the rest of the pulse up to T and finally measuring the expectation of H_{mol} .

In order to optimize for $z \in \mathcal{Z}_{ad}$, we employ the gradient descent algorithm with learning rate $\alpha_k > 0$ chosen by Armijo step rule [36]:

$$z_l^{(k+1)}(t) = z_l^{(k)}(t) - \alpha_k (\lambda z_l^{(k)}(t) + \eta_l^{(k)}(t)).$$

In order to implement the algorithm, the pulses are discretized as equidistant piecewise constant functions with $N = T/\tau \in \mathbb{N}$ steps. For this discretization, the propagator can be expressed in closed form. Let $t_n := n\tau$, $n = 0, \dots, N-1$, and set $z_l(t) := z_{l,n}$ for $t \in [t_n, t_{n+1})$, $l = 1, \dots, L$. Then for $t \in [t_n, t_{n+1})$, the propagator U takes the form

$$\begin{aligned}U(t) &= \exp(-i(t - t_n)H[z(t_n)]) \cdot \\ &\quad \cdot \exp(-i\tau H[z(t_{n-1})]) \cdots \exp(-i\tau H[z(t_0)]).\end{aligned}$$

The minimization procedure is then executed by the al-

gorithm below.

Algorithm 1: Discrete pulses VQOC algorithm

input : $z^{(0)} \in \mathbb{C}^{L \times N}$, H_{mol} , $|\psi_0\rangle$, #iterations
output: $z^{(\text{\#iterations})}$, E

for $k = 0$ **to** #iterations $- 1$ **do**

$U = S(z^{(k)});$

for $n = 1$ **to** N **do**

$P_n = -2i\Gamma(t_n, t_N)H_{\text{mol}}\Gamma(t_N, t_n)|\psi_0\rangle\langle\psi_0|;$

$\eta_{l,n}^{(k)} = \text{Tr}[Q_l^\dagger (P_n U^\dagger(t_n) + U(t_n)P_n^\dagger)];$

for $l = 1$ **to** L **do**

$z_{l,n}^{(k+1)} = z_{l,n}^{(k)} - \alpha_k (\lambda z_{l,n}^{(k)} - \eta_{l,n}^{(k)});$

end

end

end

$U_f = S(z^{(\text{\#iterations})});$

$E = \langle \psi_0 | U_f^\dagger(T) H_{\text{mol}} U_f(T) | \psi_0 \rangle;$

The total number of quantum evaluations necessary in one parameter update is given by

$$\#\text{QE} = 2 \cdot K \cdot L \cdot N \cdot \#\text{shots}. \quad (8)$$

V. RYDBERG PHYSICS

This section introduces basic Rydberg physics to identify what drift and control Hamiltonians as in Eq. (7) can look like on a Rydberg atom qubit system. This will also yield candidates for the control operators Q_l as in Eq. (IV).

The following analysis focuses on a ground-Rydberg qubit system [11]. Because the qubits never leave the \mathcal{H}^m manifold, only these states are taken into account (assuming that the system evolution time T is well below the lifetime of the states ≈ 1 s).

Assuming non-dipole coupled $|0\rangle$ and $|1\rangle$ states, the Rydberg states have a passive ‘always-on’ interaction, which can be described with a drive Hamiltonian H_d by the Van der Waals interaction [37]

$$H_d = \sum_{i=1}^m \sum_{j=1}^m \frac{C_6}{R_{ij}^6} |1\rangle_{ij} \langle 1|_{ij}, \quad (9)$$

where $R_{ij} = R|i - j|$ is the interatomic distance, with R being the nearest neighbor distance.

The coupling strength and the interaction strength are respectively characterized by the Rabi frequency Ω_R and the interaction strength $V = C_6/R^6$. This leads to two characteristic timescales $\tau_R = 1/\Omega_R$ and $\tau_V = 1/V$.

To perform single qubit manipulations on qubit j , a nearly monochromatic laser interacts with the atom to realize the Hamiltonian [38–40]

$$H_j^{01}(t) = \frac{\Omega_j(t)}{2} e^{i\varphi_j(t)} |0\rangle_j \langle 1|_j + \text{h.c.} - \Delta_j(t) |1\rangle_j \langle 1|_j, \quad (10)$$

where ‘h.c.’ refers to the hermitian conjugate of the term that precedes it. Here, $\Omega_j(t)$ [Hz] denotes the coupling strength, $\varphi_j(t)$ the phase of the laser coupled to atom j , and $\Delta_j(t) = \omega_j(t) - \omega_0$ [Hz] the detuning of the laser frequency $\omega_j(t)$ from the energy level difference ω_0 . In the current state-of-the-art systems, the control over the laser coupling $\Omega_j(t)$ and the detuning $\Delta_j(t)$ is much higher than that of the phase $\varphi_j(t)$ [41]. Therefore, often $\varphi_j(t) = \varphi_j \in [0, 2\pi)$ is taken constant. It is however not unimaginable that laser phase control will catch up in the coming years.

The control Hamiltonian H_c can contain several terms depending on which of the mentioned laser parameters can be controlled. In general, the control Hamiltonian will take the form (cf. Section IV)

$$H_c[z(t)] = \sum_{l=1}^L Q_l z_l(t) + Q_l^\dagger \overline{z_l(t)}, \quad (11)$$

where $z_l(t) \in \mathbb{C}$ [Hz], and Q_l is a m -qubit operator. The choice of $z_l(t)$ being a complex number stems from the fact that it represents both the coupling strength and

the phase in Eq. (10). However, as indicated before, the phase is often not controllable. In that case, $z_l(t) \in \mathbb{R}$ is required. This would result in

$$H_c[z] = \sum_{l=1}^L (Q_l + Q_l^\dagger) z_l,$$

where $Q_l + Q_l^\dagger$ is Hermitian. However, choosing Q_l Hermitian from the start gives

$$H_c[z] = \sum_{l=1}^L Q_l (z_l + \overline{z_l}),$$

where $z_l + \overline{z_l} \in \mathbb{R}$. Thus, if there is no control of the phase of the complex number, the formulation of Eq. (11) remains valid by choosing Q_l Hermitian.

In this part all the imaginable and realistic controls on a Rydberg system are listed, and at every future simulation it is indicated which terms are chosen to be included. For the control Hamiltonian H_c

$$H_c[z] = H_c^{\text{coup}}[z^{\text{coup}}] + H_c^{\text{det}}[z^{\text{det}}] + H_c^{\text{ent}}[z^{\text{ent}}],$$

with $z = (z^{\text{coup}}, z^{\text{det}}, z^{\text{ent}}) \in \mathcal{Z}$, $L = 2m + m(m-1)$. Here, the coupling control H_c^{coup} and detuning control H_c^{det} take the form of Eq. (11) with

$$Q_l^{\text{coup}} = |0\rangle\langle 1|_l \quad \text{and} \quad Q_l^{\text{det}} = |1\rangle\langle 1|_l$$

respectively. Notice that the coupling Hamiltonian H_c^{coup} , already allows for full control on the Bloch sphere of each individual qubit. This is why this term is also referred to as rotational control. The entanglement control is given by

$$H_c^{\text{ent}}[z] = \sum_{l=1}^m \sum_{k \neq l}^m \frac{1}{R_{lk}^6} (z_{lk} + \overline{z_{lk}}) |1\rangle_{lk} \langle 1|_{lk}. \quad (12)$$

An entanglement control could for instance be realized by tuneable Rydberg dressing [39]. In many cases, the entanglement controls will be taken equal for all interactions, such that all z_{lk} are equal for every combination of l and k .

VI. QUANTUM STRAIN

This section outlines our devised method for comparing and contrasting VQE to VQOC. When comparing VQE to VQOC, there are several factors to compare. First, the drive and control Hamiltonians in VQOC should be linked to the ansatz of VQE. Both VQE and VQOC are considered for a gr-qubit [38] Rydberg system with a passive interaction given by the Van der Waals Rydberg interaction Hamiltonian H_d , as in Eq. (9) [11]. The qubits are considered on a straight line, equidistant from one another. For VQOC only rotational control is considered ($L = m$). The hardware-efficient ansatz is considered in VQE with alternating layers of single qubit rotations and m -qubit entanglement gates U_{ent} as in Eq. (2). The assumption $\tau_V \gg \tau_R$ is made so that the hardware-efficient ansatz can physically be realized by taking $U_{ent} = \exp(-iH_d\tau_V)$. Without this assumption, too much entanglement would take place while the single qubit manipulations are happening, thus preventing them to be treated as independent. Each state on the Bloch sphere of a single qubit can be reached with a ZXZ -rotation. Such a rotation on a qubit q at a depth i can be written as

$$U_{q,i}(\vec{\theta}) = Z_{\theta_1^q,i} X_{\theta_2^q,i} Z_{\theta_3^q,i},$$

where $\vec{\theta}$ has three elements for every qubit and depth pair. For VQE, these ZXZ rotations are considered on the individual qubits in order to get analogous control to the rotational control for VQOC. We assume a Rabi frequency of $\Omega_R = 1$ kHz. This gives a gate

time $\tau_g \approx \tau_R = 1$ ms. Adhering to the condition $\tau_V \gg \tau_g$ can always realistically be done by varying R in $V = C_6/R^6$. Here we set $V = 0.1$ kHz. For the VQE algorithm then $T_{VQE} = d(\tau_g + \tau_V)$ with d the depth of the hardware-efficient ansatz. To get similar evolution we take $T_{VQOC} = T_{VQE}$.

A good quantity used to compare two quantum optimization algorithms is the strain put on the quantum computer in the total algorithm, e.g. the number of quantum evaluations that needs to be performed. This holds especially true in the NISQ era, where the availability of quantum computer power is limited. Based on Eqs. (3) and (8):

$$\frac{\#QE_{VQOC}}{\#QE_{VQE}} = K \cdot L \cdot N,$$

where K is the number of decomposition terms in the control factors ($K = 2$ in our cases), L is the number of controls scaling linearly with m ($L = m$ rotational controls in our cases), and finally, $N = T/\tau$, the number of considered time steps in VQOC, which throughout this section is fixed to 100.

Obviously, many other ansatzes for VQE, as discretizations for VQOC, are possible. The hardware-efficient ansatz and piecewise constant discretization are the most common in the literature, and we see no reason why other procedures should yield substantially different results. Nonetheless, different implementations and comparisons might yield interesting results in future research.

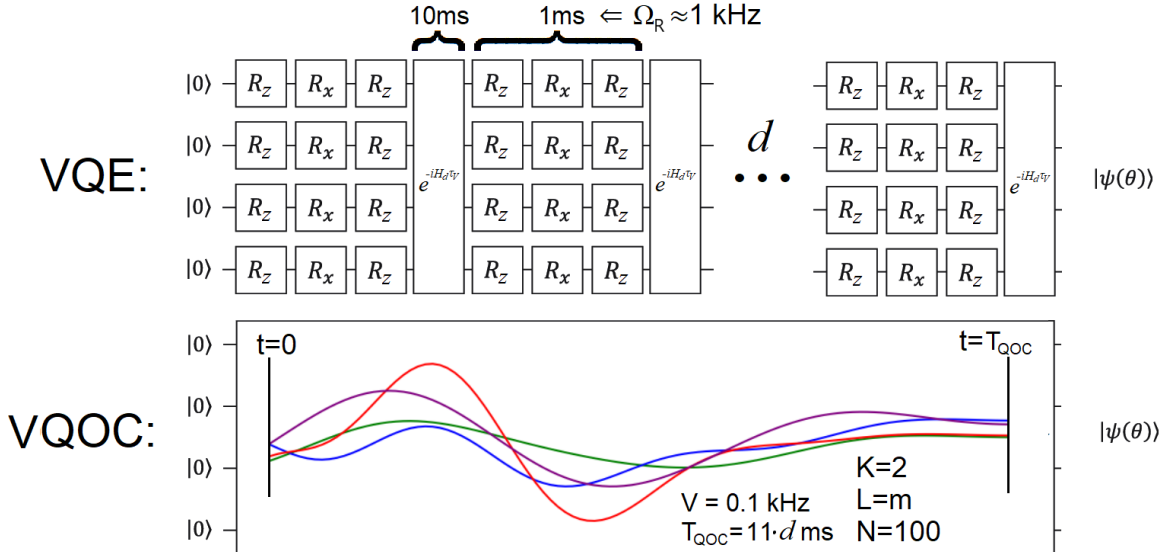


Figure 4: Layouts used to compare VQE and VQOC in the ground state energy finding problem. VQE is done on a hardware-efficient ansatz with d layers of alternating ZXZ -gates, taking time τ_g , and passive interaction via the drift Hamiltonian, for a time τ_V . VQOC is executed with piecewise constant functions consisting of N steps and $L = m$ rotational controls (giving $K = 2$). We assume $\Omega_R = 1$ kHz, leading to $\tau_g \approx 1$ ms. $\tau_V \gg \tau_g$ then leads to $\tau_V = 10$ ms which in turn gives $V = 0.1$ kHz and $T_{VQE} = T_{VQOC} = 11d$ ms.

VII. RESULTS

In this thesis, the ground state problems analyzed are LiH and H_4 . The LiH molecule is aligned on the x -axis with varying interatomic distance. The $1s$ orbital on the Li atom is fixed as fully occupied. The $2s$ and $2p_x$ orbitals of Li and the $1s$ orbitals of H are considered active. Higher energy orbitals are ignored [42]. This results, after spin and electron number reduction [26], in a 4 qubit problem. For H_4 , the atoms are aligned on the x -axis with all interatomic distances between neighboring atoms taken equal. Only the $1s$ orbitals of all 4 H atoms are considered active. This results, after spin and electron number reduction, in a 6 qubit problem [43]. The choice for these molecules as illustrating use cases is based on the fact that LiH possesses a weakly entangled ground state in the interatomic distances considered, whereas H_4 has a strongly entangled ground state here. For both these molecules, the exact H_{mol} ground state energy has

been calculated using the FCI method [42].

As a first illustration of VQOC the ground state of a LiH 4 qubit Hamiltonian is calculated for varying interatomic distances, with as initial state the vacuum state ($|\psi_0\rangle = |00\dots 0\rangle$). VQOC is run for 50 iterations with rotational control H_c^{coup} ($L = m, K = 2$), Rydberg interactions as in Eq. (9) with $C_6/R^6 = 0.1$ kHz, $T = 100$ ms and $N = 100$ [44]. The results in Fig. 5 show that VQOC is able to get below the Hartree-Fock state energy and reach chemical accuracy [18] after as few as 50 iterations in many occasions. Figure 6 shows final pulses and density matrix evolution for simulations with rotational and entanglement control as in Eq. (12) ($L = m + 1, K = 2$), Rydberg interactions with $C_6/R^6 = 0.1$ kHz, $T = 100$ ms and $N = 100$. It is shown that the density matrices are closely approximated, and the achieved energy errors, which are around 10^{-5} Hartree, are well below chemical accuracy.

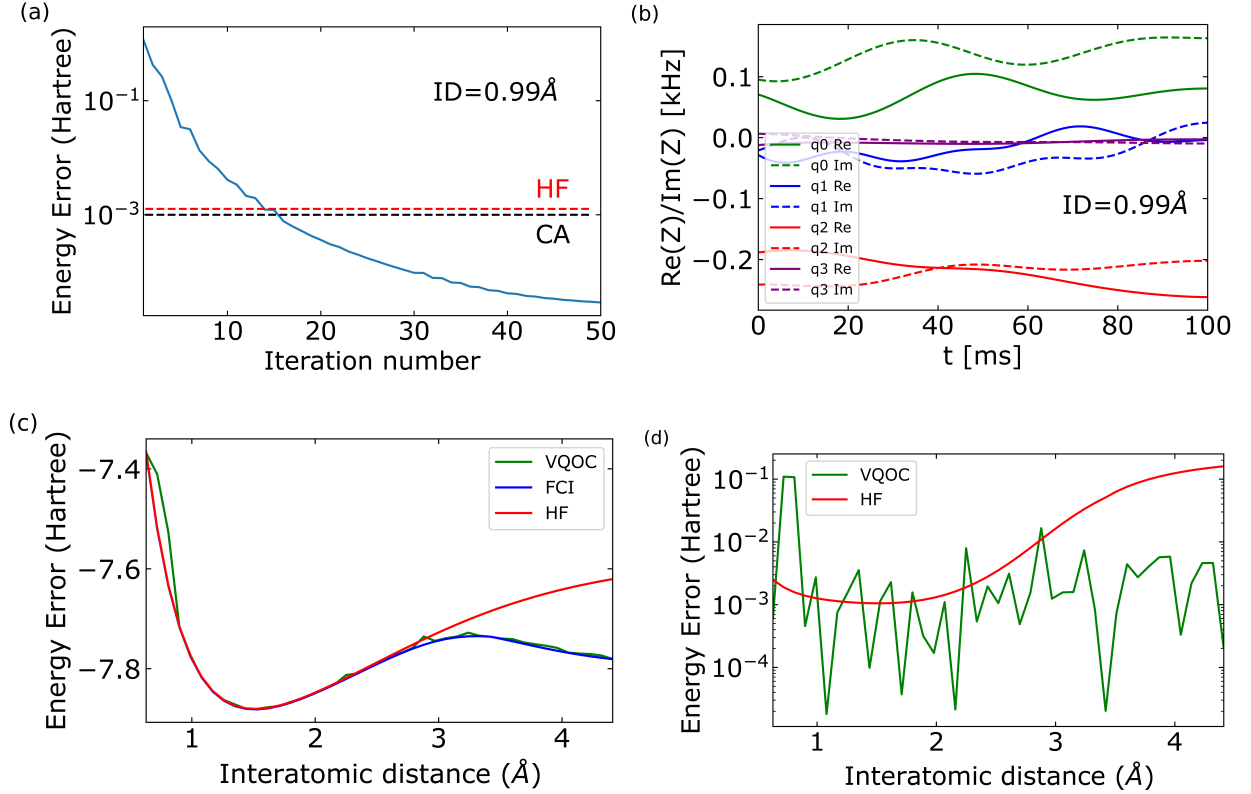


Figure 5: Simulation results of the VQOC algorithm on LiH with 4 qubits, Van der Waals drift Hamiltonian and rotational control. a) Iteration vs. energy error w.r.t. FCI ground state energy at bond length equal to 0.99\AA , together with Hartree-Fock energy and chemical accuracy. b) Finalized pulses for process of a) showing real and imaginary parts of the rotation controls on the 4 qubits. c) Bond length energy potential landscape for LiH with the FCI (exact) energy and the Hartree-Fock and VQOC energies. d) Error w.r.t. FCI ground state energy for VQOC and Hartree-Fock showing especially good results for VQOC at high bond lengths.

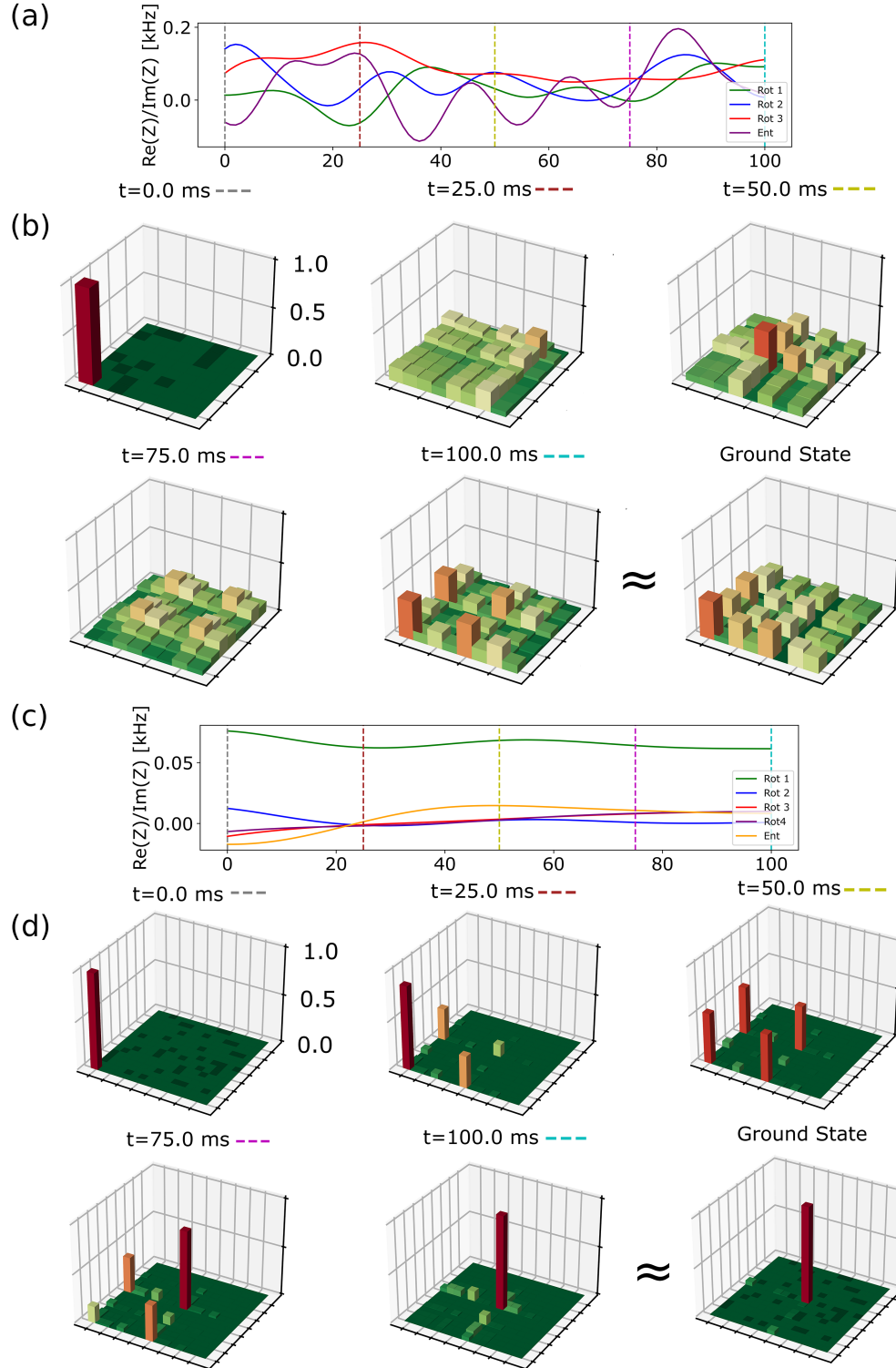


Figure 6: Ground state optimization of random $2^8 \times 2^8$ Hermitian matrix (3 qubits) and of 4 qubit LiH Hamiltonian at bond length equal to 0.99\AA , with Van der Waals drift Hamiltonian and rotational and entanglement control. a) Finalized pulses showing real part of rotation and entanglement for random Hamiltonian. b) Density matrix evolution plotted at different times during the process together with the density plot of the ground state for random Hamiltonian. c) Finalized pulses showing real part of rotation and entanglement for LiH Hamiltonian. d) Density matrix evolution plotted at different times during the process, together with the density plot of the ground state for LiH Hamiltonian.

To compare the VQE and VQOC algorithms as described in Sec. V, again LiH, but also H_4 Hamiltonians are analyzed. Figures 7 and 8 show VQE vs. VQOC results for LiH with $d = 2$, and H_4 with $d = 5$ to get $T_{VQE} = T_{VQOC} = 22$ ms and $T_{VQE} = T_{VQOC} = 55$ ms respectively. In both cases, the Hartree-Fock state is taken as an initial state [18]. At high interatomic distances VQE slightly outperforms VQOC, but from

Fig. 7d VQOC can be seen to not yet have reached full convergence. In both Fig. 7 and Fig. 8, it is seen that for low interatomic distances (Fig. 7b and Fig. 8b) VQOC converges much faster while for high interatomic distances (Fig. 7d and Fig. 8d) VQE converges much faster. In between, there are cases (Fig. 7c and Fig. 8c) for which the convergence per quantum evaluation is remarkably similar for VQE and VQOC.

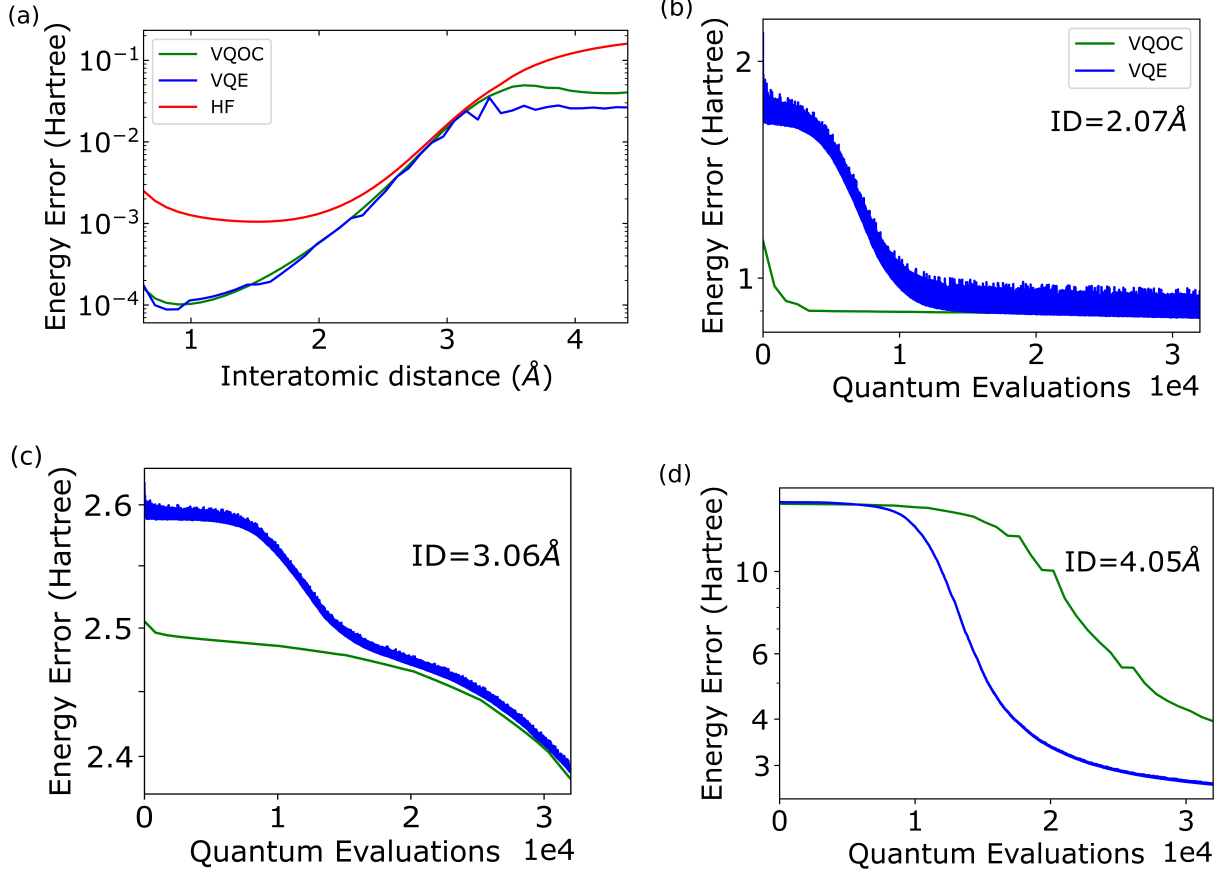


Figure 7: Comparison of VQE vs. VQOC in terms of quantum evaluations vs. energy error for LiH Hamiltonians. $d_{VQE} = 2 \Rightarrow T_{VQE} = T_{VQOC} = 22$ ms. a) Plot of final energy errors for different atomic distances after $3.2 \cdot 10^4$ quantum evaluations. b-d) Energy error vs. quantum evaluations for selected interatomic distances.

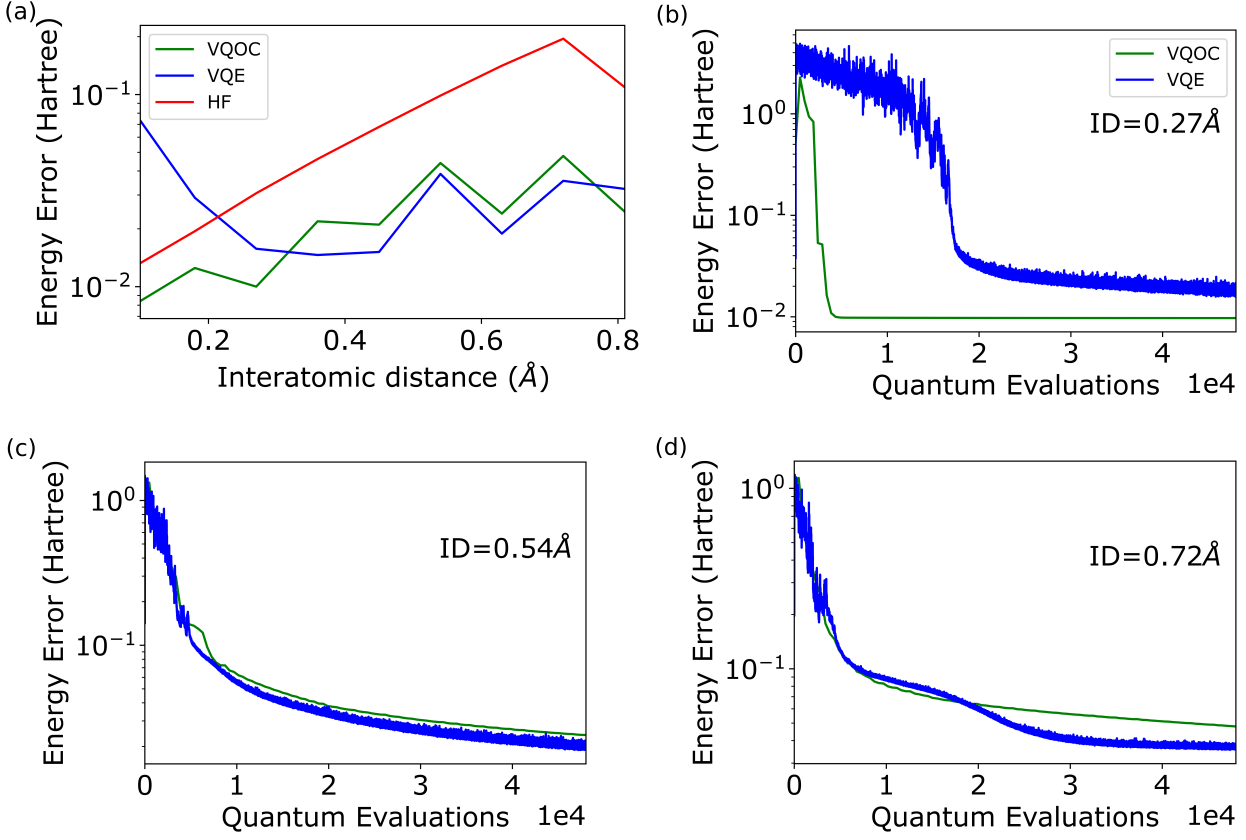


Figure 8: Comparison of VQE vs. VQOC in terms of quantum evaluations vs. energy error for H_4 Hamiltonians. $d_{VQE} = 5 \Rightarrow T_{VQE} = T_{VQOC} = 55\text{ms}$. a) Plot of final energy errors for different atomic distances after $4.8 \cdot 10^4$ quantum evaluations. b-d) Energy error vs. quantum evaluations for selected interatomic distances.

A last interesting case is when $d = 1$ giving $T_{VQE} = T_{VQOC} = 11\text{ ms}$ for H_4 . This is the case with a strongly entangled ground state and a small evolution time. This means that there is limited time to generate entanglement. Figure 9 shows the results for this case. Here the initial state is taken as the vacuum state. In Fig. 9a one can see that VQOC performs better than VQE in most

cases than. From Fig. 9b it can be seen that VQE indeed gets stuck in a local minimum, likely because the exploration of the Hilbert space is limited by the small gate sequence, whereas VQOC does much better at approximating the ground state energy. In this case, we only illustrate the convergence at one bond length, as this is representative of the results obtained for the other bond lengths.

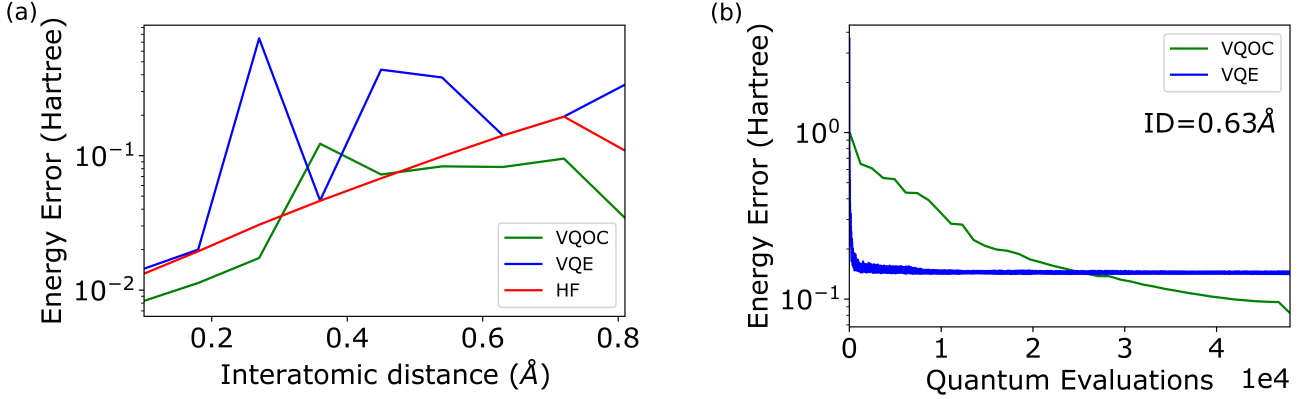


Figure 9: Comparison of VQE vs. VQOC in terms of quantum evaluations vs. energy error for H_4 Hamiltonian. $d_{VQE} = 1 \Rightarrow T_{VQE} = T_{VQOC} = 11\text{ms}$. a) Plot of final energy errors for different atomic distances after $4.8 \cdot 10^4$ quantum evaluations. b) Energy error vs. quantum evaluations for interatomic distance of 0.63\AA .

VIII. CONCLUSION

In this work, we introduce a novel pulse-based variational quantum optimal control (VQOC) algorithm for quantum chemistry applications. The method has, through simulations, shown proof of concept for a neutral atom quantum computing system with interactions between the qubits mediated via Rydberg excitations, by approximating ground state energies of simple molecules with chemical accuracy. In this process, hyperparameters like the evolution time T and the terms in the control Hamiltonian H_c were found to play important roles.

To compare VQE and VQOC is not trivial, as both algorithms use entirely different methods of optimizing. For our criteria of quantum overhead, we have shown that our VQOC method can compete with, and in certain cases outperform VQE, while doing so in a more NISQ-friendly manner. Especially, for small depths (short T) VQOC is able to outperform VQE. Especially, the better convergence of VQOC in the low evolution time regime will help stifle the influence of decoherence in NISQ era quantum computing problems. The reason for the faster convergence has to do with the accessibility of the Hilbert space, and thus with the QSL. In regimes with higher T , VQE and VQOC are able to reach very similar estimations for the ground state energy, where often for small interatomic distances VQOC performs better while for larger distances VQE is slightly better, largely due to VQOC's slower convergence in these problems. The exact reason for this behavior is not known yet, and this should be part of future research. However, we believe that VQE has an advantage at larger distances because the interatomic interactions are weaker in this regime: then the ground state is weakly entangled and VQE can immediately go to this state in one rotation. On the other hand, at small distance, the interatomic interactions are very strong, giving rise to a strongly-entangled ground state, and VQOC is able to find this state faster due to

entanglement optimization at every step.

Other points of future research would include the physical implementation of the algorithm. Several points to focus on are repeatability of the algorithm, the robustness due to errors within the pulses and the required precision of the pulses, and creating specific controlled gates as required by the parameter gradient algorithm. Another implementation issue is the matter of noise. On the pulse based level, certain noise terms can be introduced eloquently by switching to Lindbladian evolution instead of Hamiltonian [45]. A last interesting point would be to look into adapting the VQOC algorithm for qutrit or qudit manifolds [46] and its influence on barren plateaus [47, 48].

ACKNOWLEDGEMENTS

We thank Jasper Postema and Madhav Mohan for discussions. This research is financially supported by the Dutch Ministry of Economic Affairs and Climate Policy (EZK), as part of the Quantum Delta NL programme, and by the Netherlands Organisation for Scientific Research (NWO) under Grant No. 680-92-18-05.

DATA AVAILABILITY

The data that support the findings of this study are available from the corresponding author upon reasonable request.

-
- [1] A. B. Magann, C. Arenz, M. D. Grace, T.-S. Ho, R. L. Kosut, J. R. McClean, H. A. Rabitz, and M. Sarovar, *PRX Quantum* **2**, 010101 (2021).
- [2] O. R. Meitei, B. T. Gard, G. S. Barron, D. P. Pappas, S. E. Economou, E. Barnes, and N. J. Mayhall, *npj Quantum Information* **7**, 155 (2021).
- [3] A. Choquette, A. Di Paolo, P. K. Barkoutsos, D. Sénéchal, I. Tavernelli, and A. Blais, *Phys. Rev. Research* **3**, 023092 (2021).
- [4] J. Preskill, *Quantum* **2**, 79 (2018).
- [5] F. Arute, K. Arya, R. Babbush, D. Bacon, J. C. Bardin, *et al.*, *Nature* **574**, 505 (2019).
- [6] A. Kandala, A. Mezzacapo, K. Temme, M. Takita, M. Brink, J. M. Chow, and J. M. Gambetta, *Nature (London)* **549**, 242 (2017), [arXiv:1704.05018 \[quant-ph\]](#).
- [7] C. Hempel, C. Maier, J. Romero, J. McClean, T. Monz, H. Shen, P. Jurcevic, B. P. Lanyon, P. Love, R. Babbush, A. Aspuru-Guzik, R. Blatt, and C. F. Roos, *Phys. Rev. X* **8**, 031022 (2018).
- [8] A. Aspuru-Guzik and P. Walther, *Nature Physics* **8** (2012), 10.1038/nphys2253.
- [9] T. E. O'Brien, P. Rožek, and A. R. Akhmerov, *Phys. Rev. Lett.* **120**, 220504 (2018).
- [10] F. Arute, K. Arya, R. Babbush, D. Bacon, J. C. Bardin, R. Barends, *et al.*, *Science* **369**, 1084 (2020).
- [11] M. Cerezo, A. Arrasmith, R. Babbush, S. C. Benjamin, S. Endo, K. Fujii, J. R. McClean, K. Mitarai, X. Yuan, L. Cincio, and P. J. Coles, (2020), [arXiv:2012.09265 \[quant-ph\]](#).
- [12] K. Bharti, A. Cervera-Lierta, T. H. Kyaw, T. Haug, S. Alperin-Lea, A. Anand, M. Degroote, H. Heimonen, J. S. Kottmann, T. Menke, W.-K. Mok, S. Sim, L.-C. Kwek, and A. Aspuru-Guzik, *Rev. Mod. Phys.* **94**, 015004 (2022).
- [13] T. Propson, B. E. Jackson, J. Koch, Z. Manchester, and D. I. Schuster, *Phys. Rev. Applied* **17**, 014036 (2022).
- [14] S. J. Glaser, U. Boscain, T. Calarco, C. P. Koch, W. Köckenberger, R. Kosloff, I. Kuprov, B. Luy, S. Schirmer, T. Schulte-Herbrüggen, D. Sugny, and F. K. Wilhelm, *The European Physical Journal D* **69**, 279 (2015).
- [15] M. M. Müller, D. M. Reich, M. Murphy, H. Yuan, J. Vala, K. B. Whaley, T. Calarco, and C. P. Koch, *Phys. Rev. A* **84**, 042315 (2011).
- [16] N. Khaneja, T. Reiss, C. Kehlet, T. Schulte-Herbrüggen, and S. J. Glaser, *Journal of Magnetic Resonance* **172**, 296 (2005).
- [17] P. Doria, T. Calarco, and S. Montangero, *Phys. Rev. Lett.* **106**, 190501 (2011).
- [18] S. McArdle, S. Endo, A. Aspuru-Guzik, S. C. Benjamin, and X. Yuan, *Rev. Mod. Phys.* **92**, 015003 (2020).
- [19] D. J. Griffiths and D. F. Schroeter, *Introduction to quantum mechanics* (Cambridge University Press, 2020).
- [20] S. Deffner and S. Campbell, *Journal of Physics A: Mathematical and Theoretical* **50**, 453001 (2017).
- [21] M. H. Goerz, T. Calarco, and C. P. Koch, *Journal of Physics B: Atomic, Molecular and Optical Physics* **44**, 154011 (2011).
- [22] T. Caneva, M. Murphy, T. Calarco, R. Fazio, S. Montangero, V. Giovannetti, and G. E. Santoro, *Phys. Rev. Lett.* **103**, 240501 (2009).
- [23] A. Peruzzo, J. McClean, P. Shadbolt, M.-H. Yung, X.-Q. Zhou, P. J. Love, A. Aspuru-Guzik, and J. L. O'Brien, *Nature Communications* **5**, 4213 (2014), [arXiv:1304.3061 \[quant-ph\]](#).
- [24] D. A. Fedorov, B. Peng, N. Govind, and Y. Alexeev, *Materials Theory* **6**, 2 (2022).
- [25] C. Gogolin, G.-L. Anselmetti, D. Wierichs, and R. M. Parrish, *New Journal of Physics* (2021).
- [26] R. J. P. T. de Keijzer, V. E. Colussi, B. Škorić, and S. J. J. M. F. Kokkelmans, (2021), [arXiv:2102.01781 \[quant-ph\]](#).
- [27] W. M. Kirby and P. J. Love, *Phys. Rev. Lett.* **127**, 110503 (2021).
- [28] A. J. C. Woitzik, P. K. Barkoutsos, F. Wudarski, A. Buchleitner, and I. Tavernelli, *Phys. Rev. A* **102**, 042402 (2020).
- [29] J. C. Spall, *IEEE Transactions on Aerospace and Electronic Systems* **34**, 817 (1998).
- [30] O. Crawford, B. v. Straaten, D. Wang, T. Parks, E. Campbell, and S. Brierley, *Quantum* **5**, 385 (2021).
- [31] Y. Cao, J. Romero, J. P. Olson, M. Degroote, P. D. Johnson, M. Kieferová, I. D. Kivlichan, T. Menke, B. Peropadre, N. P. D. Sawaya, S. Sim, L. Veis, and A. Aspuru-Guzik, *Chemical Reviews* **119**, 10856 (2019).
- [32] L. D. Berkovitz, *Optimal control theory* (Springer, 1974).
- [33] S. P. Boyd and L. Vandenberghe, “5.5.3: Kkt optimality conditions,” in *Convex optimization* (Cambridge Univ. Pr., 2011).
- [34] L. C. Evans, *Partial differential equations*. Evans (American Mathematical Society, 1998).
- [35] M. Schuld, V. Bergholm, C. Gogolin, J. Izaac, and N. Killoran, *Phys. Rev. A* **99**, 032331 (2019).
- [36] S. Butenko and P. M. Pardalos, *Numerical Methods and Optimization: An introduction* (CRC Press, 2015).
- [37] X.-F. Shi and Y. Lu, *Phys. Rev. A* **104**, 012615 (2021).
- [38] M. Morgado and S. Whitlock, *AVS Quantum Science* **3**, 023501 (2021), <https://doi.org/10.1116/5.0036562>.
- [39] M. Saffman, *Journal of Physics B: Atomic, Molecular and Optical Physics* **49**, 202001 (2016).
- [40] C. S. Adams, J. D. Pritchard, and J. P. Shaffer, *Journal of Physics B: Atomic, Molecular and Optical Physics* **53**, 012002 (2019).
- [41] J. Zha, Z. Qin, J. Yan, N. Cao, Q. Wei, and P. Wang, *Results in Physics* **22**, 103594 (2021).
- [42] D. McQuarrie, *Quantum Chemistry*, v. 1 (University Science Books, 2008) Chap. 10, pp. 266–290.
- [43] In this work the molecular Hamiltonians have been determined in the STO-3G basis using quantum computation libraries *OpenFermion* [49] and *Psi4* [50].
- [44] In this work all VQOC simulations have been performed using Python Library QuTiP [51] while the VQE calculations have been performed using MATLAB R2019b [52].
- [45] B. Li, S. Ahmed, S. Saraogi, N. Lambert, F. Nori, A. Pitchford, and N. Shammah, *Quantum* **6**, 630 (2022).
- [46] J. R. Weggemans, A. Urech, A. Rausch, R. Spreuw, R. Boucherie, F. Schreck, K. Schoutens, J. Minář, and F. Speelman, (2021), [arXiv:2106.11672 \[quant-ph\]](#).
- [47] J. R. McClean, S. Boixo, V. N. Smelyanskiy, R. Babbush, and H. Neven, *Nature Communications* **9**, 4812 (2018).
- [48] A. Uvarov, J. D. Biamonte, and D. Yudin, *Phys. Rev. B* **102**, 075104 (2020).

- [49] J. R. McClean, K. J. Sung, I. D. Kivlichan, Y. Cao, C. Dai, E. Schuyler Fried, C. Gidney, B. Gimby, P. Gokhale, T. Häner, T. Hardikar, V. Havlíček, O. Higgott, C. Huang, *et al.*, arXiv e-prints , arXiv:1710.07629 (2017), [arXiv:1710.07629 \[quant-ph\]](#).
- [50] D. G. A. Smith, L. A. Burns, A. C. Simmonett, R. M. Parrish, M. C. Schieber, R. Galvelis, P. Kraus, H. Kruse, R. Di Remigio, A. Alenaizan, A. M. James, *et al.*, [The Journal of Chemical Physics](#) **152**, 184108 (2020), <https://doi.org/10.1063/5.0006002>.
- [51] J. Johansson, P. Nation, and F. Nori, [Computer Physics Communications](#) **183**, 1760–1772 (2012).
- [52] MATLAB, *version 9.7.0.1216025 (R2019b)* (The MathWorks Inc., Natick, Massachusetts, 2019).